Numerical Evaluation of Blood Flow and Heat Transfer of Non-Newtonian Fluid in a Vertical Artery with Atherosclerosis



By:

Majid Hussain Shah

Reg. No. 951-FBAS/MSMA/F23

Department of Mathematics and Statistics
Faculty of Sciences
International Islamic University, Islamabad
Pakistan
2025

Numerical Evaluation of Blood Flow and Heat Transfer of Non-Newtonian Fluid in a Vertical Artery with Atherosclerosis



By:

Majid Hussain Shah Reg. No. 951-FBAS/MSMA/F23

Supervised By:

Prof. Dr. Rahmat Ellahi

Department of Mathematics and Statistics
Faculty of Sciences
International Islamic University, Islamabad
Pakistan
2025

Numerical Evaluation of Blood Flow and Heat Transfer of Non-Newtonian Fluid in a Vertical Artery with Atherosclerosis

By:

Majid Hussain Shah

Reg. No. 951-FBAS/MSMA/F23

A Thesis

Submitted in the Partial Fulfillment of the

Requirements for Degree of

MASTER OF SCIENCE

IN

MATHEMATICS

Supervised By:

Prof. Dr. Rahmat Ellahi

Department of Mathematics and Statistics
Faculty of Sciences
International Islamic University, Islamabad
Pakistan
2025

DEDICATION

I express my heartfelt gratitude and utmost respect as I dedicated this work to my beloved

PROPHET MUHAMMAD

(صلى الله عليه وآله وسلم)

and

Prof. Ahmad Zeeshan

My respected teacher.

He has consistently inspired and uplifted me, leading me to pursue higher goals in life.

DECLARATION

I declare that this thesis is entirely my own work, except where I have clearly acknowledged the contributions of others. This thesis has not been submitted for any other academic award.

| Date | | |
|------|--|--|
| | | |
| | | |

Majid Hussain Shah MS in Mathematics 951-FBAS/MSMA/F23 ACKNOWLEDGEMENTS

In the name of Allah, the Most Gracious, the Most Merciful. First and foremost, I

express my sincere gratitude to Almighty Allah for providing me with guidance,

knowledge, and the strength to undertake this study and complete it successfully.

I am deeply grateful to my respected teacher and supervisor, Prof. Dr. Rahmat Ellahi,

for his invaluable guidance and support throughout this work. I would also like to

acknowledge Prof. Dr. Nasir Ali, Chairperson of the Department of Mathematics and

Statistics at IIUI, for providing the necessary resources to carry out this research.

My heartfelt thanks go to my esteemed teacher, Prof. Dr. Ahmad Zeeshan, for his

continuous encouragement, valuable insights, and helpful suggestions during this

research journey. His support and feedback have been crucial to the successful

completion of this dissertation.

I am also indebted to my parents, teachers, and siblings for their unwavering support,

encouragement, and genuine interest in my academic achievements. Their prayers and

best wishes have always been a source of strength for me in all aspects of my life. I

would especially like to thank my father Ijaz Hussain Shah and my brothers Hammad

Ahmed Shah and Sajjad Ahmad Shah for their consistent moral support.

Mr. Majid Hussain Shah

951-FBAS/MSMA/F23

iii

PREFACE

Arterial blood flow is defined by unsteady, pulsatile flow governed by the values of the Womersley number along with the ratio of inertial forces of the blood flow to viscous forces. For a normal flow, the flow is laminar, but with the occurrence of secondary flows due to disturbances such as arterial curves and bifurcations. Stenosis, which refers to the narrowing of the artery, can interfere with normal flow, induce turbulence, and result in severe conditions such as thrombosis. Increased shear stress at the site of stenosis has the potential to activate platelets, risking complete blockage. It is crucial to understand this hemodynamics for diagnostics, surgical planning, and medical device design.

Understanding blood flow under diseases such as stenosis will be critical for guiding efficient diagnosis, treatment, and medical device development. This is because narrower arteries can cause circulation disruption, increase shear stress, and lead to consequences like thrombosis or heart attacks [1]. The research into blood flow dynamics of stenosed arteries has gained more attention from researchers over the last century. Jamil et al. [2] examined the flow of blood through a stenosed, inclined artery in a magnetic field by simulating blood as a Casson fluid. Patel and Patel [3] examined the blood circulation in a stenosed artery using the fractional derivative for time. A precise description of the temperature fields, magnetic particle velocity, and blood velocity is obtained by expressing the set of governing equations. Majeed et al. [4] observed heat and mass transfer by blood circulation containing magnetic particles through a cylindrical tube. Moreover, Jamil et al. [5] examined non-Newtonian magnetic blood flow with thermal radiation through an inclined artery. Tabi et al. [6] examined a mathematical representation of blood flow when magnetic particles are present. Luqman et al. [7] evaluated OHAM's performance in the analysis of how

thermal radiation and magnetic fields affect blood flow inside cylindrical arteries. Yakubu et al. [8] examined how the temperature distribution and blood velocity vary in a straight circular cylindrical tube. Kot and Elmaboud [9] analyzed the unsteady flow of a hybrid nano fluid, which is used to simulate blood dynamics, through a mild constricted artery. The work represented blood as a non-Newtonian fluid to capture the effects of gyrotactic microorganism motion in the bloodstream, providing a more accurate understanding of complicated biofluid behavior. Raju et al. [10] focused on examining the blood flow containing gold particles in two different geometries of stenosed arteries by taking the effect of periodic body acceleration. Abbas et al. [11] examined the unsteady circulation of blood in a constricted artery with body acceleration and an externally applied magnetic field. The biomathematical examination of blood flow in constricted tapering arteries was conducted by Akber, N S. [12]. To explore the important impacts of increasing blood velocity and associated hemodynamic stresses on the vascular endothelium (inner lining of arteries) in dogs, Fry, D. L. [13] employed an intra-aortic device to induce controlled increments in turbulence and shear stress. The researchers employed hydrodynamic modelling and histologic study to find a critical shear stress level of 379 ± 85 dynes/cm2, above which endothelial cells quickly exhibited evidence of structural injury, including cytoplasmic swelling, nuclear deformation, and erosion. The findings emphasize how mechanical forces, such as turbulence and laminar shear stress, can disturb endothelial homeostasis; how hemodynamic factors play a causative role in vascular diseases such as atherosclerosis.

Subsequently, physicians have been able to study blood flow in patients with clinical devices such as Doppler ultrasound and angiography. These studies support earlier findings that plagues generally develop in areas of low shear stress instead of high shear

stress under conditions of steady flow. Ku et al. [14] indicated that significant oscillations in the wall shear direction may enhance atherogenesis.

Early detection and treatment of heart disease depend on the understanding of blood circulation in constricted arteries. As a non-Newtonian fluid and examining how it behaves via the constricted arteries, the work provides significant understanding of how different physiological parameters affect flow characteristics. The findings can be utilized in the development of next-generation biomedical devices, such as MEMS-based flow sensors, which could offer a non-invasive means of monitoring restenosis. This could significantly reduce repeated procedures and improve long-term patient care.

The main objective of our research is to simulate and examine blood circulation in a constricted artery by considering Bingham fluid. The goal is to simulate the Bingham plastic fluid flow in a symmetric stenotic artery. Provide graphical visualization of the following parameters: flow rate, flow resistance, wall shear stress, axial velocity, and temperature distribution. Through the application of the finite difference method to model and visualize flow characteristics during variable physiological conditions, to analyze the physical effect of stenosis on blood circulation.

This thesis comprises three chapters. Details are as follows:

Chapter one deals with preliminarily that will be used in subsequent chapters. Chapter two treats computational biomedical simulations of hybrid nanoparticles on unsteady blood hemodynamic in a stenotic artery. Chapter three is on numerical evaluation of blood flow and heat transfer of non-Newtonian fluid in a vertical artery with atherosclerosis.

Table of Contents

| Chapter 1 | 1 |
|---|----|
| Basic Definitions | 1 |
| 1.1 Introduction | 1 |
| 1.2 Medical background and terminology | 2 |
| 1.3 Governing equations for incompressible fluid flow | 4 |
| 1.3.1 Continuity equation for incompressible fluid | 4 |
| 1.3.2 Momentum equation for incompressible fluid | 4 |
| 1.3.3 Energy equation for incompressible fluid | 5 |
| 1.3.4 Bingham plastic model and papanastasiou regularization | 5 |
| 1.4 Numerical techniques | 6 |
| 1.5 Significance of blood flow modeling | 6 |
| Chapter 2 | 7 |
| Computational Biomedical Simulations of Hybrid Nanoparticles on Unst Hemodynamic in a Stenotic Artery | • |
| 2.1 Introduction | 7 |
| 2.2 Geometry of the problem | 8 |
| 2.3 Governing equations | 8 |
| 2.4 Numerical approach | 11 |
| 2.5 Stability Criteria | 13 |
| 2.6 Results and discussion | 13 |
| 2.7 Conclusion | 18 |
| Chapter 3 | 20 |
| Numerical Evaluation of Blood Flow and Heat Transfer of Non-Newtonia Vertical Artery with Atherosclerosis | |
| 3.1 Introduction | |
| 3.2 Problem formulation | 20 |
| 3.3 Finite difference approximation | 26 |
| 3.4 Stability Criteria | 26 |
| 3.5 Results and discussion | 27 |
| 3.6 Conclusion | 32 |

List of Figures

| Fig.2. 1: Geometry of the problem | 8 |
|--|----|
| Fig.2. 2: Velocity profile for β | 16 |
| Fig.2. 3: Velocity profile for η | 16 |
| Fig.2. 4: Velocity profile for ws. | 16 |
| Fig.2. 5: Velocity profile for m, $\beta = 0.5$. | 16 |
| Fig.2. 6: Temperature profile for β. | 17 |
| Fig.2. 7: Temperature profile for $m, \beta = 0.5$. | 17 |
| Fig.2. 8: Wall shear stress for β. | 17 |
| Fig.2. 9: Flow rate for β. | 17 |
| Fig.2. 10: Resistance impedance. | 18 |
| Fig.3. 1: Geometries of the problem. | 21 |
| Fig.3. 2: Velocity profile for <i>Gr</i> . | 29 |
| Fig.3. 3: Wall Shear Stress for <i>Gr</i> . | 29 |
| Fig.3. 4: Flow rate for <i>Gr</i> | 29 |
| Fig.3. 5: Resistive impedance for <i>Gr</i> | 29 |
| Fig.3. 6: Velocity profile for Ma , $Gr = 0.5$. | 30 |
| Fig.3. 7: Wall shear stress for <i>Ma</i> | 30 |
| Fig.3. 8: Flow rate for Ma , $Gr = 0.5$ | 30 |
| Fig.3. 9: Resistive impedance for <i>Ma</i> | 30 |
| Fig.3. 10: Velocity profile for <i>Bn</i> | 31 |
| Fig.3. 11: Resistive impedance for <i>Bn</i> . | 31 |
| Fig.3. 12: Temperature profile for <i>Nr</i> . | 31 |
| Fig 3 13: Temperature profile for <i>Ec</i> | 31 |

Chapter 1

Basic Definitions

1.1 Introduction

Fluids are usually classified in two categories one is Newtonian, and the other one is non-Newtonian fluids in fluid mechanics. For instance, gasoline, alcohol, and water are considered Newtonian fluids because they follow Newton's law of viscosity. On the other hand, Paint, ketchup, honey, blood, and other non-Newtonian fluids do not have the linear relationship. Although exhibiting a fluid-like character, blood exhibits complex rheological behavior similar to that of a non-Newtonian fluid, especially upon variation in shear conditions, because it has suspended elements such as red and white blood cells.

A fundamental understanding of blood flow is necessary in order to know how cardiovascular conditions impact human health. Arteries, veins, and the heart constitute the circulatory system, functioning together to facilitate the flow of oxygenated as well as deoxygenated blood. Blood from the body enters the right atrium through the superior as well as inferior vena cava. After passing through the tricuspid valve and into the right ventricle, then it is pumped into the pulmonary arteries and after that into the lungs to receive oxygen. After returning via the pulmonary veins to the left atrium, oxygen-rich blood enters the left ventricle by the bicuspid (mitral) valve. Ultimately, the aortic valve and the aorta pump it to the remainder of the body. Any constriction of the arteries disrupts this critical mechanism, reducing blood flow and raising the risk of significant cardiovascular problems.

Coronary heart disease, particularly the formation of stenosis by atherosclerosis, disrupts blood flow and results in serious cardiac conditions such as heart attacks. Although a common treatment involves angioplasty with stent implantation, the issue of restenosis, wherein the artery again narrows following treatment, is still a serious problem. Current methods of detecting restenosis involve invasive procedures, which are accompanied by further health risks and cannot be used in real-time applications. A non-invasive, real-time, and reliable solution is required for improved patient outcomes. Effective design of these solutions requires an understanding of the circulation of blood in constricted arteries by considering the non-Newtonian behaviors of blood.

The modeling of blood circulation in constricted arteries by utilizing the Bingham fluid model is our main research goal. The artery is supposed to be stenotic, simulating actual pathological situations. In the mathematical modelling of our problem, continuity, momentum, and energy equations are included for cylindrical coordinates. MATLAB is used for computational results and to analyze the outcomes in tabular and graphical form. It allows a comprehensive analysis of how different parameters affect blood circulation, especially when stenosis in the arteries is present.

1.2 Medical background and terminology

In this chapter an essential background of this work is provided. This chapter includes biological experiments of terminology, literature surveys, general equations, and solution methodology. This research purpose is to model the motion of blood in constricted arteries as a result of stenosis, when the buildup of plaque influences effective blood flow. The plaque comprises fat, cholesterol, and other chemicals and blocks blood from flowing into the heart. Chronic plaque deposition, also called atherosclerosis, can narrow the inner diameter of the artery, leading to serious impairment of blood flow. Heart attacks are the major cause of mortality in US adults,

primarily due to blockage of coronary arteries through atherosclerosis. Here, the plaque ruptures or becomes dislodged, creating a blood clot (thrombus) that blocks the artery. Acute occlusion may lead to a lethal heart attack. Understanding of blood circulation in constricted arteries is significant for the prediction and development of disease as well as identify effective diagnostic and treatment techniques. The outcome of this research will contribute to the biomedical engineering field by incorporating principles from fluid dynamics, with the implications to stent design, and surgical planning.

Angioplasty is one of the most common treatments for reopening clogged arteries that have narrowed. In this minimally invasive surgery, a balloon catheter is inserted and expanded to reopen the artery, and a stent or a mesh tube is usually put in to keep the artery open. Restenosis (re-blocking of the arteries) can occur after stent insertion, particularly in those with underlying disorders. Restenosis is often discovered by more invasive testing, which increases the danger and pain. A more realistic method is to combine MEMS with stents. A tiny tracker can be attached to the stent to wirelessly send information to medical staff about things like blood pressure or flow rate. Repeated procedures would not be necessary if restenosis were to be identified early because of this non-invasive monitoring. Nevertheless, there are major engineering challenges in creating such a device. In order to be inserted into the artery without obstructing blood flow, the sensor would have to be small enough. Additionally, due to their size and safety issues, traditional battery-powered devices are complex. Utilizing the blood flow itself to power is a more realistic approach. Saving energy aside, a passive sensor design that would only report back when it senses an external signal will make the system simpler, safer, and more reliable.

1.3 Governing equations for incompressible fluid flow

To learn more about how blood moves through constricted arteries, scientists began utilizing mathematical models in the 1970s and 1980s. These models made assumptions about Newtonian fluid dynamics, vessel walls, and steady flow. They also used simple designs, such as tubes with circular or elliptical narrowing. By using this method, researchers were able to develop practical equations that characterize blood flow patterns [15,16]. Blood is frequently represented as an incompressible fluid, which means that its density does not change while it flows. Such fluid motion is governed by the following basic equations:

1.3.1 Continuity equation for incompressible fluid

According to the continuity equation, across a control volume, the total mass flux is equal to the rate of mass change within that volume [17].

$$\nabla \cdot \mathbf{V} = 0. \tag{1.1}$$

Where V is velocity, under the assumption of incompressibility, this holds for Newtonian and non-Newtonian fluids.

1.3.2 Momentum equation for incompressible fluid

Sum of all forces acting on fluid is equal to its rate of change of momentum.

$$\rho\left(\frac{\partial \mathbf{v}}{\partial t} + (\mathbf{V} \cdot \nabla)\mathbf{V}\right) = -\nabla p + \mu \nabla^2 \mathbf{V} + f. \tag{1.2}$$

 $\rho\left(\frac{\partial \mathbf{V}}{\partial t} + (\mathbf{V} \cdot \nabla)\mathbf{V}\right)$ is inertial force, pressure gradient is presented by ∇p , $\mu \nabla^2 \mathbf{V}$ is viscous forces, and f is a body force.

Because of its nearly constant viscosity and linear shear-stress-strain-rate connection, blood is frequently considered a Newtonian fluid when flowing in large arteries. While in a diseased artery, blood behaves like a non-Newtonian fluid due to its variable viscosity in diseased region.

1.3.3 Energy equation for incompressible fluid

In bioheat modelling and fluid dynamics, the energy equation controls the temperature change in a flowing fluid. When there is incompressible Newtonian flow, such as blood in large arteries, convection and conduction cause changes in thermal energy.

$$\rho c_p \left(\frac{\partial T}{\partial t} + V \nabla T \right) = k \nabla^2 T. \tag{1.3}$$

Where T is temperature, density is ρ , specific heat is c_p , k represent thermal conductivity, and V is velocity. This equation illustrates the conservation of thermal energy; conduction and internal heat creation from viscosity are on the right side, while unsteady and convective heat transfer are on the left.

1.3.4 Bingham plastic model and papanastasiou regularization

Fluids that act like rigid bodies under low stress but flow like viscous fluids when a yield stress is exceeded are described by the Bingham plastic model.

$$\begin{cases} A_1 = 0, & S \le \tau_y \\ S = \left[\mu_o + \frac{\tau_y}{\gamma}\right] A_1, & S > \tau_y \end{cases}$$
 (1.4)

when $S \le \tau_y$ this introduces singularity, which complicates the numerical simulation. To address this, Papanastasiou, T. C. [18] proposed regularization which is

$$S = \left[\mu_o + \tau_y \frac{(1 - e^{-m|\gamma|})}{\gamma}\right] A_1. \tag{1.5}$$

Where m is a regularization parameter ($m = 100 \sim 1000$), this model ensures numerical stability.

1.4 Numerical techniques

For those situations where analytical solutions are impossible, numerical methods play a key role in modeling blood flow in representative approximations of vascular geometries. Through these methods, complex, pulsatile, and the Navier-Stokes equations can be solved to analyze non-Newtonian flow using discretization of the domain. One of the early methods that can be used for simple geometries with structured grids is the Finite Difference Method (FDM). To understand wall shear stress and pressure distribution, it has been effectively applied to simulate blood circulation in stenosed arteries under pulsatile flow conditions [19].

1.5 Significance of blood flow modeling

A number of studies show the significance of blood circulation modeling in the arteries to understand cardiovascular physiology and analyze disease development. It is commonly known that complicated geometries and different vessel wall characteristics affect arterial blood flow, which is unsteady. Mathematical models can capture these dynamics, and they can provide us with information on wall shear stress, pressure gradient, as well as flow rate. Such modeling facilitates the creation of medical equipment and diagnostic tools while offering an easy method to study circulatory activity.

Chapter 2

Computational Biomedical Simulations of Hybrid Nanoparticles on Unsteady Blood Hemodynamic in a Stenotic Artery

2.1 Introduction

In this chapter, we discuss how hybrid nanoparticles (Ag–Al₂O₃) affect blood circulation within a constricted artery. First, the governing equations for blood flow are converted into a dimensionless form and then solved numerically using a finite difference method, considering the assumption of mild stenosis. From our analysis of the hybrid silver–aluminum oxide nanoparticles, we observed that these particles help lower resistance to flow. We also examine the effects of other factors, such as the slip parameter (w_s), variable viscosity (η_0), and the nanoparticle shape factor (m), on the velocity and temperature profiles of blood. Further, source/sink parameter also affects the flow and discovers that they can significantly impact blood dynamics. Through this study, our simulations will help us to understand how these nanoparticles might improve blood flow in patients with artery blockages.

2.2 Geometry of the problem

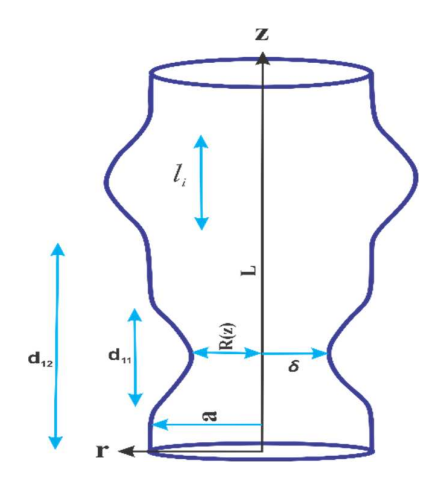


Fig. 2. 1: Geometry of the problem.

We model blood moving through the artery as unsteady, laminar, incompressible, and axisymmetric. To describe the artery's geometry, we use cylindrical coordinates (r, θ, z) . The artery's radius R(z) is defined by a piecewise function so that it covers both the normal and aneurysmal sections.

$$\bar{R}(\bar{z}) = \begin{cases}
(a + \bar{z}^* \bar{z}) \left(1 - \left(\frac{\delta^*}{2a}\right) \left(1 + \cos\left(\frac{2\pi}{l_i}\right) \left(\bar{z} - d_{1i} - \left(\frac{l_i}{2}\right)\right)\right)\right), d_{1i} \leq \bar{z} \leq d_{1i} + l_i, \\
(a + \bar{z}^* \bar{z}), & otherwise
\end{cases} \tag{2.1}$$

here, d_{1i} is the axial location of the center of the i^{th} aneurysmal region, length is l_i of the aneurysmal region, normal artery radius is a, the tapering parameter is z^* , height of the aneurysm δ^* . Stenosis ($\delta^* > 0$), and Aneurysm ($\delta^* < 0$).

2.3 Governing equations

In an artery with stenosis and aneurysms, the temperature and velocity fields for the unsteady blood flow are as follows:

$$V = [u(r, z, t), 0, w(r, z, t)], T = T(r, z, t).$$
(2.2)

Here, u(r, z, t) is the radial velocity component and w(r, z, t) is the axial component.

$$\frac{\partial \bar{u}}{\partial \bar{r}} + \frac{\bar{u}}{\bar{r}} + \frac{\partial \bar{w}}{\partial \bar{z}} = 0, \tag{2.3}$$

$$\rho_{hnf}\left(\frac{\partial \overline{u}}{\partial \overline{t}} + \overline{w}\frac{\partial \overline{u}}{\partial \overline{z}} + \overline{u}\frac{\partial \overline{u}}{\partial \overline{r}}\right) = -\frac{\partial P}{\partial \overline{r}} + \left(\frac{\partial}{\partial \overline{z}}(S_{\overline{r}\overline{z}}) + \frac{1}{\overline{r}}\frac{\partial}{\partial \overline{r}}(\overline{r}S_{\overline{r}\overline{r}})\right),\tag{2.4}$$

$$\rho_{hnf}\left(\frac{\partial \overline{w}}{\partial \overline{t}} + \overline{w}\frac{\partial \overline{w}}{\partial \overline{z}} + \overline{u}\frac{\partial \overline{w}}{\partial \overline{r}}\right) = -\frac{\partial P}{\partial \overline{z}} + \left(\frac{\partial}{\partial \overline{z}}(S_{\overline{z}\overline{z}}) + \frac{1}{\overline{r}}\frac{\partial}{\partial \overline{r}}(\overline{r}S_{\overline{r}\overline{z}})\right) + \tag{2.5}$$

$$(\rho \gamma)_{hnf} g(T-T_1)$$
,

$$\left(\rho C_p\right)_{hnf} \left(\frac{\partial T}{\partial \bar{t}} + \bar{w} \frac{\partial T}{\partial \bar{z}} + \bar{u} \frac{\partial T}{\partial \bar{r}}\right) = k_{hnf} \left(\frac{\partial^2 T}{\partial \bar{r}^2} + \frac{1}{\bar{r}} \frac{\partial T}{\partial \bar{r}} + \frac{\partial^2 T}{\partial \bar{z}^2}\right) + Q_0. \tag{2.6}$$

where

$$S_{\overline{r}\overline{r}} = 2 \frac{\partial \overline{u}}{\partial \overline{r}} \mu_{hnf}, S_{\overline{z}\overline{z}} = 2 \frac{\partial \overline{w}}{\partial \overline{z}} \mu_{hnf}, \text{ and } S_{\overline{r}\overline{z}} = \mu_{hnf} \left(\frac{\partial \overline{u}}{\partial \overline{z}} + \frac{\partial \overline{w}}{\partial \overline{r}} \right).$$

The heat absorption or generation constant parameter is Q_0 , hybrid nanofluid viscosity is μ_{hnf} , k_{hnf} present thermal conductivity, the density is ρ_{hnf} , thermal expansion coefficient is $(\rho \gamma)_{hnf}$, and heat capacitance is $(\rho C_p)_{hnf}$.

The above equations are converted into dimensionless form using the following transformations:

$$r = \frac{\bar{r}}{a}, z = \frac{\bar{z}}{l_{0}}, w = \frac{\bar{w}}{U_{0}}, R = \frac{\bar{R}}{a}, p = \frac{Pa^{2}}{U_{0}l_{0}\mu_{0}}, u = \frac{l_{0}\bar{u}}{\delta^{*}U_{0}}, \theta = \frac{T-T_{1}}{T_{w}-T_{1}}, S_{rr} = \frac{l_{0}}{U_{0}\mu_{0}}S_{\bar{r}\bar{r}}, S_{zz} = \frac{l_{0}}{U_{0}\mu_{0}}S_{\bar{z}\bar{z}}, S_{rz} = \frac{a}{U_{0}\mu_{0}}S_{\bar{r}\bar{z}}, t = \frac{U_{0}\bar{t}}{a}, Gr = \frac{ga^{2}r\rho_{f}}{U_{0}\mu_{f}}(T_{w} - T_{1}), Pr = \frac{C_{p}\mu_{f}}{k_{f}}, Re = \frac{U_{0}a\rho_{f}}{\mu_{f}}, \beta = \frac{Q_{0}ak_{f}}{T_{w}-T}, \overline{w}_{S} = \frac{w_{S}}{U_{0}}.$$

When we put these dimensionless variables into the equations, while assuming $\frac{\delta^*}{R_0} \ll 1$ and $\frac{R_0}{l_0} \approx O(1)$, the resulting system becomes:

$$\frac{\partial w}{\partial z} = 0 , \qquad (2.8)$$

$$\frac{\partial p}{\partial r} = 0 , \qquad (2.9)$$

$$\frac{\rho_{hnf}}{\rho_f} Re \frac{\partial w}{\partial t} = -\frac{\partial P}{\partial z} + \frac{1 - \eta_o \theta}{(1 - \phi_1)^{2.5} (1 - \phi_2)^{2.5}} \left(\frac{1}{r} \frac{\partial w}{\partial r} + \frac{\partial^2 w}{\partial r^2} \right) + \frac{(\rho \gamma)_{hnf}}{(\rho \gamma)_f} G_r \theta, \tag{2.10}$$

$$Pr \, Re \, \frac{(\rho c_p)_{hnf}}{(\rho c_p)_f} \frac{k_{hnf}}{k_f} \frac{\partial \theta}{\partial t} = \left(\frac{1}{r} \frac{\partial \theta}{\partial r} + \frac{\partial^2 \theta}{\partial r^2}\right) + \frac{k_f}{k_{hnf}} \beta. \tag{2.11}$$

The pulsatile pressure gradient is defined as

$$-\frac{\partial P}{\partial z} = A_{11} + A_{22}\cos(\omega_p t) , \quad t > 0.$$
 (2.12)

Here, A_{11} is the constant (steady) component of the pressure gradient, A_{22} represents the pressure oscillation that raises systolic and diastolic pressures, and pulse rate frequency is ω_p . When converted to dimensionless form, this same pressure gradient becomes,

$$-\frac{\partial P}{\partial z} = B_1[1 + e\cos(c_1 t)].$$

Where $e = \frac{A_{22}}{A_{11}}$, and $B_1 = \frac{A_{11}R_0^2}{\mu_0U_0}$. Below are the equations for volumetric flow rate, wall shear stress, and flow resistance.

$$\tau_s = -\mu_f \left(\frac{\partial w}{\partial r}\right)_{r=R} , \qquad (2.13)$$

$$Q_F = 2\pi \int_0^R w \, r \, dr \, , \qquad (2.14)$$

$$\lambda = \frac{L\left(\frac{\partial P}{\partial z}\right)}{Q_F} \,, \tag{2.15}$$

where

$$R(z) = (1 + z \zeta) \left(1 - \frac{\delta}{2} \left(1 + \cos 2\pi \left(z - d_i - \frac{1}{2} \right) \right) \right), d \le z \le d + 1,$$
 (2.16)

with

$$d_i = \frac{\mathbf{z}_i}{l_i}$$
, $\zeta = \frac{\zeta^* l_i}{a}$.

To utilize the effect of geometry we used transformation $\left(x = \frac{r}{R(z)}\right)$.

$$\frac{\rho_{hnf}}{\rho_f} Re \frac{\partial w}{\partial t} = B_1 [1 + e \cos(c_1 t)] + \frac{1 - \eta_0 \theta}{(1 - \phi_1)^{2.5} (1 - \phi_2)^{2.5}} \frac{1}{R^2} \left(\frac{1}{x} \frac{\partial w}{\partial x} + \frac{\partial^2 w}{\partial x^2} \right) + \tag{2.17}$$

$$\frac{(\rho\gamma)_{hnf}}{(\rho\gamma)_f}G_r\theta$$
,

$$Pr Re \frac{(\rho c_p)_{hnf}}{(\rho c_p)_f} \frac{k_{hnf}}{k_f} \frac{\partial \theta}{\partial t} = \frac{1}{R^2} \left(\frac{1}{r} \frac{\partial \theta}{\partial r} + \frac{\partial^2 \theta}{\partial r^2} \right) + \frac{k_f}{k_{hnf}} \beta . \tag{2.18}$$

$$\tau_{s} = -\frac{1}{R} \left(\frac{\partial w}{\partial x} \right)_{x=1} \,, \tag{2.19}$$

$$Q_F = 2\pi R^2 \int_0^1 w \, x \, dx \,, \tag{2.20}$$

$$\lambda = \frac{L\left(\frac{\partial P}{\partial z}\right)}{Q_E},\tag{2.21}$$

where,

$$R(z) = (1 + z\zeta) \left(1 - \left(1 + \cos 2\pi \left(z - d_i - \frac{1}{2}\right)\right) \frac{\delta}{2}\right), d \le z \le d + 1,$$
 (2.22)

with

$$d_i = \frac{\mathbf{z}_i}{l_i}$$
, $\zeta = \frac{\zeta^* l_i}{a}$.

2.4 Numerical approach

The FTCS approach, is used to compute the partial differential equations numerically. FTCS is utilized because it is simple and reliable in computational fluid dynamics; the

procedure first discretises the spatial domain. Subsequently, for each node x_i at time t_j , the velocity component w is computed. The method uses central differencing for the spatial derivatives (second-order accurate) and forward differencing for time to ensure stability and efficiency.

$$\frac{\partial w}{\partial t} \cong \frac{w_{i,j+1} - w_{i,j}}{\Delta t},\tag{2.23}$$

$$\frac{\partial w}{\partial x} \cong \frac{w_{i+1,j} - w_{i-1,j}}{2\Delta x},\tag{2.24}$$

$$\frac{\partial^2 w}{\partial x^2} \cong \frac{w_{i+1,j} - 2w_{i,j} + w_{i-1,j}}{\Delta x^2},\tag{2.25}$$

$$\frac{\rho_{hnf}}{\rho_f} = \phi_2 \frac{\rho_{s2}}{\rho_f} + \left((1 - \phi_1) + \phi_1 \frac{\rho_{s1}}{\rho_f} \right) (1 - \phi_2) , \qquad (2.26)$$

$$\frac{(\rho\gamma)_{hnf}}{(\rho\gamma)_f} = \phi_2 \frac{(\rho\gamma)_{s2}}{(\rho\gamma)_f} + \left((1 - \phi_1) + \phi_1 \frac{(\rho\gamma)_{s1}}{(\rho\gamma)_f} \right) (1 - \phi_2) , \qquad (2.27)$$

$$\frac{(\rho c_p)_{hnf}}{(\rho c_p)_f} = \phi_2 \frac{(\rho c_p)_{s2}}{(\rho c_p)_f} + \left((1 - \phi_1) + \phi_1 \frac{(\rho c_p)_{s1}}{(\rho c_p)_f} \right) (1 - \phi_2) , \qquad (2.28)$$

$$\frac{k_{hnf}}{k_f} = \frac{k_{s2} + (m-1)k_f - (m-1)\phi_2(k_f - k_{s2})}{k_{s2} + (m-1)k_f + \phi_2(k_f - k_{s2})} \frac{k_{s1} + (m-1)k_f + \phi_2(k_f - k_{s1})}{k_{s1} + (m-1)k_f - (m-1)\phi_2(k_f - k_{s1})},$$
(2.29)

$$w_{i,j+1} = w_{i,j} + \frac{\Delta t \left[B_1 \left[1 + e \cos(c_1 t_j) \right] + \frac{1 - \eta_0 \theta_{i,j}}{(1 - \phi_1)^{2.5} (1 - \phi_2)^{2.5}} \frac{1}{R^2} \left(\frac{1}{x_i} w_x + w_{xx} \right) + \left(\frac{(\rho \gamma)_{hnf}}{(\rho \gamma)_f} \right) G_r \theta_{i,j} \right]}{\left(\frac{\rho_{hnf}}{\rho_f} \right) Re} ,$$
(2.30)

$$\theta_{i,j+1} = \theta_{i,j} + \frac{\Delta t \frac{k_{hnf}}{k_f} \left[\frac{1}{\Pr R^2 Re} \left(\frac{1}{x_i} \theta_x + \theta_{xx} \right) + \frac{k_f}{k_{hnf}} \beta \right]}{\frac{(\rho c_p)_{hnf}}{(\rho c_p)_f}}.$$
(2.31)

Boundary conditions are:

$$w_{i}^{1} = \theta_{i}^{1} = 0 \text{ at } t = 0,$$

$$w_{i+1}^{j} = w_{i}^{j}, \theta_{i+1}^{j} = \theta_{i}^{j} \text{ at } x = 0,$$

$$w_{N+1}^{j} = 0, \theta_{N+1}^{j} = 1, \text{ at } x = 1.$$
(2.31)

2.5 Stability Criteria

Numerical method starts with spatial domain discretising into N+1 grid points, by taking step size of $\Delta x = 1/(N+1)$. Velocity component is computed over specific instances t_j at each of these spatial positions, where $t_j = (k-1) \Delta t$ and Δt denotes the time. Stability of this method is highly sensitive to choice Δx and Δt . $\Delta x = 0.025$ and $\Delta t = 0.00001$ were chosen after various numerical experiments, as these step sizes ensure a consistent and stable solution.

2.6 Results and discussion

Velocity profiles for various values of β and η_0 are shown in Figs. (2.2) and (2.3). The plots indicate the same behaviour for both parameters: the velocity increases for both parameters β and η_0 . This indicates that the velocity is increasing both parameters. Physically, this means that increased values of β and η_0 decrease the blood's viscosity,

or in other words, reduce the internal resistance between particles. Figs. (2.4) and (2.5) show how the slip parameter (w_s) and nanoparticle shape (m) affect velocity profiles. The findings indicate, velocity increases by increasing w_s as well as m, e.g., from bricks to cylinders or platelets. Such properties can be useful in the optimization of blood circulation during medical interventions.

Figs. (2.6) and (2.7) show how β and m influence the temperature profiles. They exhibit a similar trend; temperature rises as either β or m rises. Physically, a greater β means that there is stronger internal heat generation (source) or weaker heat absorption (sink), resulting in higher temperatures. The shape parameter m characterizes the geometry of nanoparticles that are dispersed in blood. When m increases, meaning that particles are more complicated, non-spherical, thermal conductivity increases, and temperature profiles increase. This shows how the shape of nanoparticles is essential in increasing the transport of heat, particularly in areas of unusual arterial structure such as stenoses and aneurysms.

Fig. (2.8) demonstrates how wall shear stress effected by variations in β . Graph shows wall shear stress increases significantly with increasing β . In Fig. (2.8), this trend is easily observable. Physically, the flow near the artery wall is enhanced by raising β , especially in a stenosed region. Wall shear stress increased due to enhancing velocity gradients. In Fig. (2.9), the impact of β on blood particles' volumetric flow rate is displayed. The graph shows a similar as the velocity profiles show an increasing function.

Fig. (2.10) illustrates the outcomes of resistance to flow. In equation (2.21), relationship of impedance and flow rate is defined, revealed the inverse relationship of resistance to flow with flow rate, and that is why these data are moving in the reverse direction of

flow rate as predicted. Each outcome is calculated for hybrid nanofluid. It is well understood that with any increase in any of the parameters $(\beta, \eta_o, and Gr)$, the impedance data follow a decreasing trend that is contrary to flow rate.

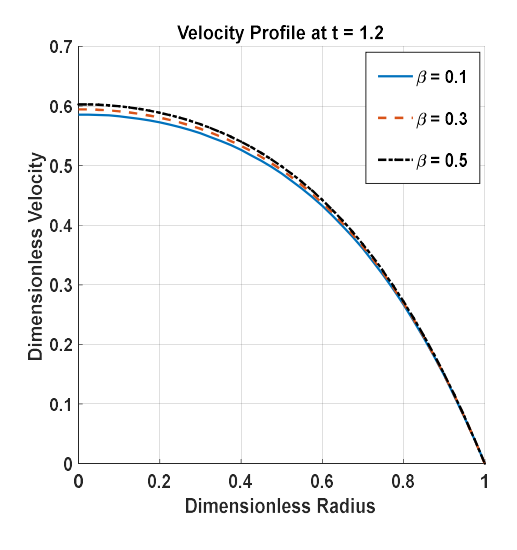


Fig.2. 2: Velocity profile for β .

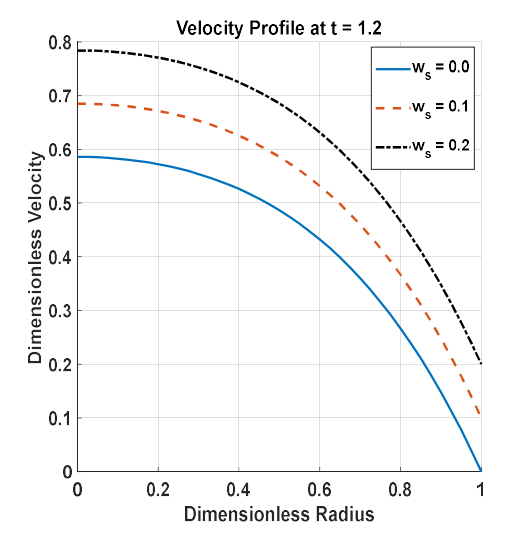


Fig.2. 4: Velocity profile for w_s.

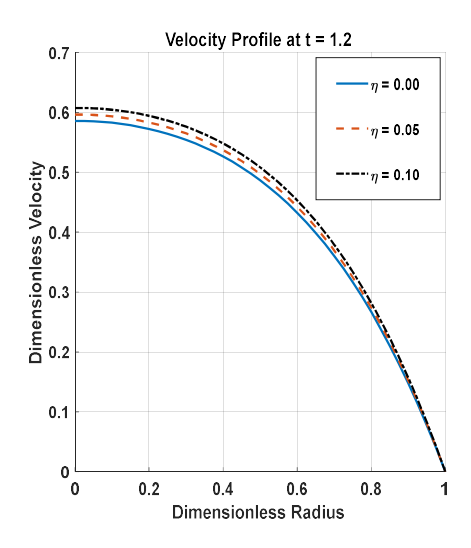


Fig.2. 3: Velocity profile for η .

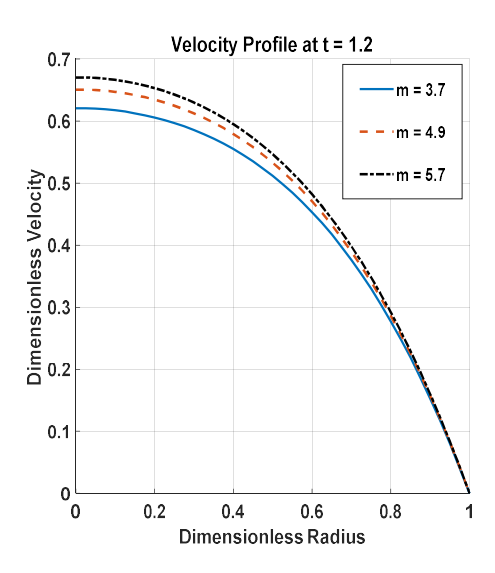


Fig.2. 5: Velocity profile for m, $\beta = 0.5$.

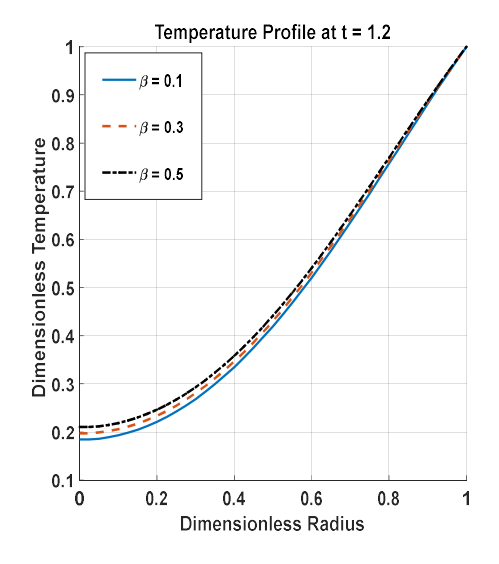
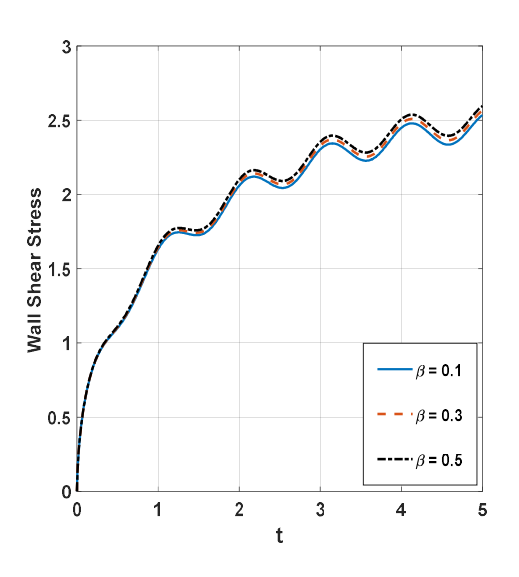


Fig.2. 6: Temperature profile for β .

Fig. 2. 7: Temperature profile for m, $\beta = 0.5$.



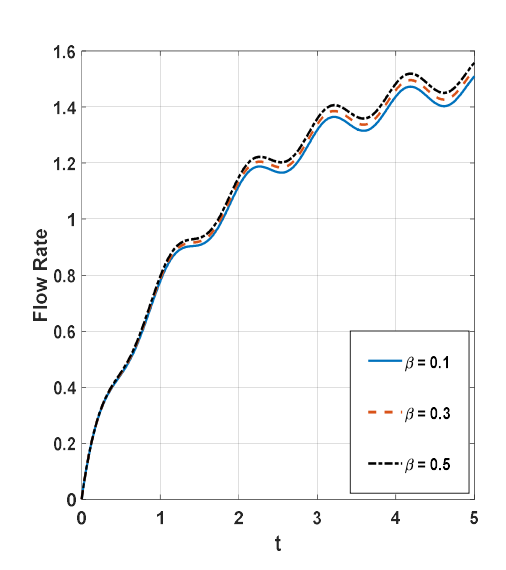


Fig.2. 8: Wall shear stress for β .

Fig.2. 9: Flow rate for β .

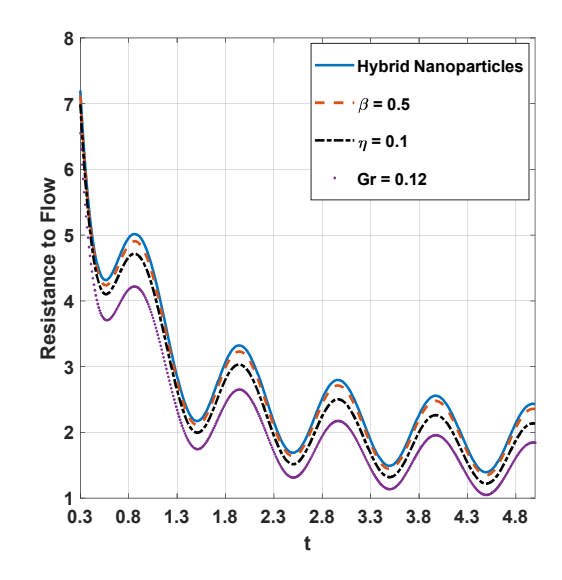


Fig.2. 10: Resistance impedance.

2.7 Conclusion

In this research, parametric impact of hybrid nanofluid flow $(Ag - Al_2O_3/blood)$ through a stenosed artery is examined. Here are some significant findings about hemodynamic and thermal dynamics under varying physical conditions:

- The hybrid nanofluid's velocity profiles are positively impacted by an increase in the slip parameter (w_s) , variable viscosity (η_0) , source/sink strength (β) , and nanoparticle shape factor (m). The flow performance is improved by platelet-shaped particles.
- The addition of hybrid nanoparticles helps improve flow dynamics, as indicated by the rise in wall shear stress with β and Grashof number (Gr).
- Increasing β results in a significant increase in blood flow rate, suggesting that source-driven acceleration may positively impact flow behavior in stenotic regions.

- As β , η_0 , and Gr increase, the resistance to flow decreases, showing an inverse pattern with flow rate and helping to promote smoother circulation.
- The rise in temperature profiles with β and nanoparticle shape factor (m) highlights how non-spherical nanoparticles can improve thermal conductivity.

These findings support the possibility of improving blood flow and temperature control through the optimization of nanoparticle shape, viscosity fluctuation, and boundary slip, providing new information for biological applications in cardiovascular treatments.

Chapter 3

Numerical Evaluation of Blood Flow and Heat Transfer of Non-Newtonian Fluid in a Vertical Artery with Atherosclerosis

3.1 Introduction

In the biological sciences, it is crucial to experimentally and theoretically predict blood flow in stenosed arteries. Although humankind has greatly benefited from the groundbreaking discoveries and advancements in medicine and medical sciences, cardiovascular illnesses continue to be the leading cause of death, even in developed countries. Atherosclerosis promotes due to low-density lipoprotein, a chronic inflammatory reaction in the artery walls caused by the accumulation of macrophage white blood cells. Plaque, therefore, develops in the arterial blood vessels' interior walls. The current work examines the unsteady blood flow by using Bingham fluid in a vertical stenosed artery with effect of magnetic field. Flow equations are investigated in a cylindrical coordinate system. Governing equations are computed numerically by explicit finite difference approach. The effects of different parameters are shown graphically and discussed in detail.

3.2 Problem formulation

We study the unsteady, incompressible, pulsatile flow through vertically artery. The Bingham fluid model is used to analyze blood flow. Cylindrical coordinates (r, θ, z) are used to express radial, circumference, and direction of flow. In Fig. (3.1) geometries are shown.

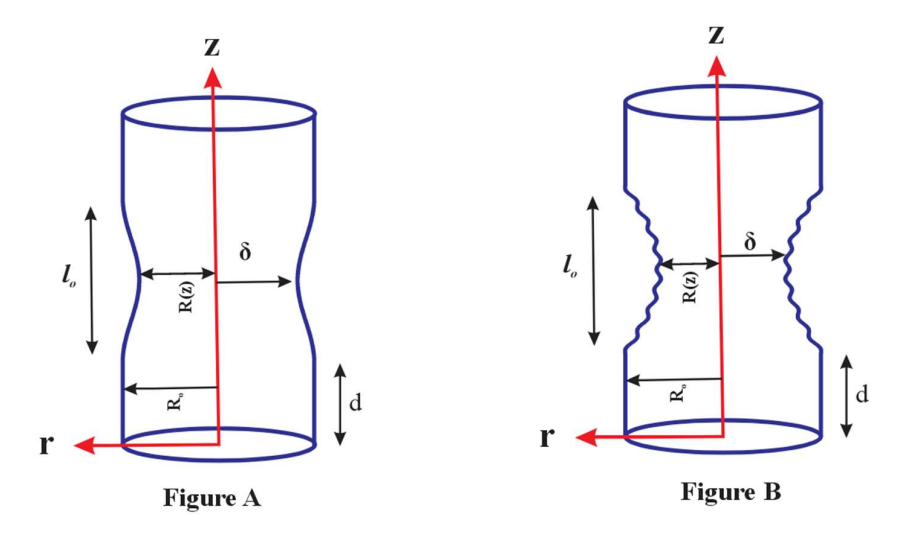


Fig. 3. 1: Geometries of the problem.

Smooth stenosis is shown in figure. A.

$$R(z) = \begin{cases} R_o - \left(1 + \cos\left(\frac{2\pi}{l_o}\right)\left(\bar{z} - \bar{d} - \left(\frac{l_o}{2}\right)\right)\right)\left(\frac{\delta}{2}\right), \bar{d} \leq \bar{z} \leq \bar{d} + l_o \\ R_o, & otherwise \end{cases}$$
(3.1)

Irregular stenosis is shown in figure. B.

$$R(z) = \begin{cases} R_o - 2\delta \left[\cos \left(2\pi \left(\frac{\bar{z} - \bar{d}}{2} - \frac{l_o}{4} \right) \right) - \frac{7}{100} \cos \left(\left(\bar{z} - \bar{d} - \frac{l_o}{2} \right) 17\pi \right) \right], \bar{d} < \bar{z} < \bar{d} + l_o \\ R_o, \end{cases}$$
 otherwise (3.2)

In these equations, R_o is radius of artery without stenosis, axial coordinate is presented by \bar{z} , R(z) is radius, \bar{d} is region where stenosis starts, height is δ , and length of stenosis is l_o . As flow is axisymmetric, the circumferential direction is neglected.

We have used the Bingham fluid model to analyze blood flow. Cauchy stress tensor is:

$$T = -pI + \tau. (3.3)$$

Where pI is spherical and S is deviatoric part of T. A simplified rheological relationship for Bingham fluid is,

$$\begin{cases} A_1 = 0, & S \le \tau_y \\ S = \left[\mu_o + \frac{\tau_y}{\gamma}\right] A_1, & S > \tau_y \end{cases}$$
 (3.4)

If $\tau_y \ge \tau$ then $\gamma = 0$ and there will be a $\frac{0}{0}$ form generate. But in our model, we are using only the case when $\tau_y \le S$ but we will face a singularity in our problem when $\tau_y = S$, To address this problem, we used Papanastasiou's regularization to resolve the singularity in the model.

$$S = \left[\mu_o + \tau_y \frac{(1 - e^{-m|\gamma|})}{\gamma}\right] A_1. \tag{3.5}$$

When $m \to \infty$, our problem becomes the $S = \left[\mu_o + \frac{\tau_y}{\gamma}\right] A_1$, but we won't take m so large that it makes our problem one from the past when singularity will occur. We will take m so large that it will have a significant enough effect on our problem to address the singularity with little difference to the results.

Rate of strain and deformation tensor are:

$$\gamma = \sqrt{\frac{1}{2} tr(A_1^2)}, A_1 = (\nabla V)^T + (\nabla V)$$
 respectively.

Governing equations are:

$$\frac{\partial \overline{u}}{\partial r} + \frac{\overline{u}}{r} + \frac{\partial \overline{w}}{\partial \overline{z}} = 0 , \qquad (3.6)$$

$$\rho\left(\frac{\partial \overline{u}}{\partial \overline{t}} + \overline{w}\frac{\partial \overline{u}}{\partial \overline{z}} + \overline{u}\frac{\partial \overline{u}}{\partial \overline{r}}\right) = -\frac{\partial P}{\partial \overline{r}} + \left(\frac{\partial}{\partial \overline{z}}(S_{\overline{r}\overline{z}}) + \frac{1}{\overline{r}}\frac{\partial}{\partial \overline{r}}(\overline{r}S_{\overline{r}\overline{r}})\right),\tag{3.7}$$

$$\rho\left(\frac{\partial \overline{w}}{\partial \overline{t}} + \overline{w}\frac{\partial \overline{w}}{\partial \overline{z}} + \overline{u}\frac{\partial \overline{w}}{\partial \overline{r}}\right) = -\frac{\partial P}{\partial \overline{z}} + \left(\frac{\partial}{\partial \overline{z}}(S_{\overline{z}\overline{z}}) + \frac{1}{\overline{r}}\frac{\partial}{\partial \overline{r}}(\overline{r}S_{\overline{r}\overline{z}})\right) + \rho g\beta(T - T_1)$$
(3.8)

 $\sigma B_o^2 \overline{w}$,

$$\left(\rho C_p\right) \left(\frac{\partial T}{\partial \bar{t}} + \bar{w} \frac{\partial T}{\partial \bar{z}} + \bar{u} \frac{\partial T}{\partial \bar{r}}\right) = k \left(\frac{\partial^2 T}{\partial \bar{r}^2} + \frac{1}{\bar{r}} \frac{\partial T}{\partial \bar{r}} + \frac{\partial^2 T}{\partial \bar{z}^2}\right) - \frac{\partial q_r}{\partial \bar{r}} + \sigma B_o^2 \bar{w}^2 . \tag{3.9}$$

Associated boundary conditions are:

$$\overline{w}(R,t) = 0, \frac{\partial \overline{w}(0,t)}{\partial \overline{r}} = 0, \overline{w}(r,0) = 0,$$

$$T(R,t) = 1, \frac{\partial T(0,t)}{\partial \overline{r}} = 0, T(r,0) = 0.$$
(3.10)

 $S_{\overline{rz}}$, $S_{\overline{zz}}$, and $S_{\overline{rr}}$ are tangential, axial, and radial stress of Bingham fluid respectively.

$$S_{\overline{r}\overline{r}} = 2 \frac{\partial \overline{u}}{\partial \overline{r}} \left[\mu_0 + \frac{\tau_y \left(1 - e^{-m\sqrt{\left(\frac{\partial \overline{u}}{\partial \overline{z}} + \frac{\partial \overline{w}}{\partial \overline{r}}\right)^2 + 2\left(\left(\frac{\partial \overline{u}}{\partial \overline{r}}\right)^2 + \left(\frac{\overline{u}}{\overline{r}}\right)^2 + \left(\frac{\partial \overline{w}}{\partial \overline{z}}\right)^2\right)}{\sqrt{\left(\frac{\partial \overline{u}}{\partial \overline{z}} + \frac{\partial \overline{w}}{\partial \overline{r}}\right)^2 + 2\left(\left(\frac{\partial \overline{u}}{\partial \overline{r}}\right)^2 + \left(\frac{\overline{u}}{\overline{r}}\right)^2 + \left(\frac{\partial \overline{w}}{\partial \overline{z}}\right)^2\right)}} \right]},$$
(3.11)

$$S_{\overline{z}\overline{z}} = 2 \frac{\partial \overline{w}}{\partial \overline{z}} \left[\mu_0 + \frac{\tau_y \left(1 - e^{-m \sqrt{\left(\frac{\partial \overline{u}}{\partial \overline{z}} + \frac{\partial \overline{w}}{\partial \overline{r}} \right)^2 + 2\left(\left(\frac{\partial \overline{u}}{\partial \overline{r}} \right)^2 + \left(\frac{\overline{u}}{\overline{r}} \right)^2 + \left(\frac{\partial \overline{w}}{\partial \overline{z}} \right)^2 \right)}{\sqrt{\left(\frac{\partial \overline{u}}{\partial \overline{z}} + \frac{\partial \overline{w}}{\partial \overline{r}} \right)^2 + 2\left(\left(\frac{\partial \overline{u}}{\partial \overline{r}} \right)^2 + \left(\frac{\overline{u}}{\overline{r}} \right)^2 + \left(\frac{\partial \overline{w}}{\partial \overline{z}} \right)^2 \right)}} \right]},$$
(3.12)

$$S_{\overline{r}\overline{z}} = \left(\frac{\partial \overline{u}}{\partial \overline{z}} + \frac{\partial \overline{w}}{\partial \overline{r}}\right) \left[\mu_0 + \frac{\tau_y \left(1 - e^{-m\sqrt{\left(\frac{\partial \overline{u}}{\partial \overline{z}} + \frac{\partial \overline{w}}{\partial \overline{r}}\right)^2 + 2\left(\left(\frac{\partial \overline{u}}{\partial \overline{r}}\right)^2 + \left(\frac{\overline{u}}{\overline{r}}\right)^2 + \left(\frac{\partial \overline{w}}{\partial \overline{z}}\right)^2\right)}{\sqrt{\left(\frac{\partial \overline{u}}{\partial \overline{z}} + \frac{\partial \overline{w}}{\partial \overline{r}}\right)^2 + 2\left(\left(\frac{\partial \overline{u}}{\partial \overline{r}}\right)^2 + \left(\frac{\overline{u}}{\overline{r}}\right)^2 + \left(\frac{\partial \overline{w}}{\partial \overline{z}}\right)^2\right)}} \right]}.$$
(3.13)

Where $P, k, \rho, T, \mu, g, t, C_p, \sigma, and \beta$ represents pressure, thermal conductivity, density, temperature, dynamic viscosity, gravitational acceleration, time, specific heat capacity, electrical conductivity, and thermal expansion.

Here, $q_r = -\frac{3\sigma^*}{4k^*} \left(\frac{\partial T^4}{\partial \bar{r}} \right)$ is radiative heat flux.

The nondimensional variables are introduced by Tripathi et al. [20]

$$r = \frac{\bar{r}}{R_0}, R = \frac{\bar{R}}{R_0}, d = \frac{\bar{d}}{l_0}, w = \frac{\bar{w}}{U_0}, p = \frac{PR_0^2}{U_0 l_0 \mu_0}, z = \frac{\bar{z}}{l_0}, u = \frac{l_0 \bar{u}}{\delta^* U_0},$$

$$\theta = \frac{T - T_1}{T_w - T_1}, S_{rr} = \frac{l_0}{U_0 \mu_0} S_{\overline{rr}}, S_{zz} = \frac{l_0}{U_0 \mu_0} S_{\overline{zz}}, S_{rz} = \frac{R_0}{U_0 \mu_0} S_{\overline{rz}}, t = \frac{U_0 \bar{t}}{R_0}.$$
(3.14)

Using the variables mentioned above and the hypotheses $\frac{\delta^*}{R_0} \ll 1$ and $\frac{R_0}{l_0} \approx O(1)$, the pulsatile pressure gradient presented by Handford, S. W. [21] is:

$$-\frac{\partial P}{\partial z} = A_{11} + A_{22} \cos(\omega_p t) , t > 0 .$$
 (3.15)

In which ω_p is the pulse rate frequency, A_{11} represents steady pressure gradient, A_{22} represents pressure oscillation that raises systolic and diastolic pressures.

In dimensionless form Pressure gradient is:

$$-\frac{\partial P}{\partial z} = B_1 [1 + e \cos(c_1 t)]. \tag{3.16}$$

Where $e = \frac{A_{22}}{A_{11}}$, and $B_1 = \frac{A_{11}R_0^2}{\mu_0U_0}$. The flow equations in dimensionless form are

expressed as follows:

$$\frac{\partial w}{\partial z} = 0 , \qquad (3.17)$$

$$\frac{\partial p}{\partial r} = 0 , (3.18)$$

$$Re\frac{\partial w}{\partial t} = \frac{1}{r}\frac{\partial}{\partial r}\left(r\left(\frac{\partial w}{\partial r} + B_n\left(1 - e^{-M\left|\frac{\partial w}{\partial r}\right|}\right)\right)\right) + G_r\theta - M_a^2w + B_1[1 + G_r\theta]$$
(3.19)

 $e\cos(c_1t)$],

$$\frac{\partial \theta}{\partial t} = \frac{1}{\Pr{Re}} \left(\frac{1}{r} \frac{\partial \theta}{\partial r} + \frac{\partial^2 \theta}{\partial r^2} \right) + \frac{Nr}{\Pr{Re}} \frac{\partial^2 \theta}{\partial r^2} + \frac{Ec \, M_a^2}{Re} w^2 \,, \tag{3.20}$$

$$S_{rz} = \left(\frac{\partial w}{\partial r} + B_n \left(1 - e^{-M\left|\frac{\partial w}{\partial r}\right|}\right)\right). \tag{3.21}$$

In non-dimensional form geometry is:

$$R(z) = \begin{cases} 1 - \left(1 + \cos 2\pi \left(z - d - \frac{1}{2}\right)\right) \frac{\delta^*}{2}, d \le z \le d + 1. \\ 0 \text{ otherwise} \end{cases}$$
 (3.22)

To utilize the effect of geometry we used transformation $\left(x = \frac{r}{R(z)}\right)$.

$$Re\frac{\partial w}{\partial t} = \frac{1}{x R^2} \frac{\partial}{\partial x} \left(x \left(\frac{\partial w}{\partial x} + RB_n \left(1 - e^{-\frac{M}{R} \left| \frac{\partial w}{\partial x} \right|} \right) \right) \right) + G_r \theta - M_a^2 w + B_1 \left[1 + \frac{1}{2} \left(\frac{\partial w}{\partial x} + \frac{\partial w}{\partial x} \right) \right] + C_r \theta - M_a^2 w + B_1 \left[1 + \frac{1}{2} \left(\frac{\partial w}{\partial x} + \frac{\partial w}{\partial x} \right) \right] + C_r \theta - M_a^2 w + B_1 \left[1 + \frac{1}{2} \left(\frac{\partial w}{\partial x} + \frac{\partial w}{\partial x} \right) \right] + C_r \theta - M_a^2 w + B_1 \left[1 + \frac{\partial w}{\partial x} \right] + C_r \theta - M_a^2 w + B_1 \left[1 + \frac{\partial w}{\partial x} \right] + C_r \theta - M_a^2 w + B_1 \left[1 + \frac{\partial w}{\partial x} \right] + C_r \theta - M_a^2 w + B_1 \left[1 + \frac{\partial w}{\partial x} \right] + C_r \theta - M_a^2 w + B_1 \left[1 + \frac{\partial w}{\partial x} \right] + C_r \theta - M_a^2 w + B_1 \left[1 + \frac{\partial w}{\partial x} \right] + C_r \theta - M_a^2 w + B_1 \left[1 + \frac{\partial w}{\partial x} \right] + C_r \theta - M_a^2 w + B_1 \left[1 + \frac{\partial w}{\partial x} \right] + C_r \theta - M_a^2 w + B_1 \left[1 + \frac{\partial w}{\partial x} \right] + C_r \theta - M_a^2 w + B_1 \left[1 + \frac{\partial w}{\partial x} \right] + C_r \theta - M_a^2 w + B_1 \left[1 + \frac{\partial w}{\partial x} \right] + C_r \theta - M_a^2 w + B_1 \left[1 + \frac{\partial w}{\partial x} \right] + C_r \theta - M_a^2 w + B_1 \left[1 + \frac{\partial w}{\partial x} \right] + C_r \theta - M_a^2 w + B_1 \left[1 + \frac{\partial w}{\partial x} \right] + C_r \theta - M_a^2 w + B_1 \left[1 + \frac{\partial w}{\partial x} \right] + C_r \theta - M_a^2 w + B_1 \left[1 + \frac{\partial w}{\partial x} \right] + C_r \theta - M_a^2 w + B_1 \left[1 + \frac{\partial w}{\partial x} \right] + C_r \theta - M_a^2 w + B_1 \left[1 + \frac{\partial w}{\partial x} \right] + C_r \theta - M_a^2 w + B_1 \left[1 + \frac{\partial w}{\partial x} \right] + C_r \theta - M_a^2 w + B_1 \left[1 + \frac{\partial w}{\partial x} \right] + C_r \theta - M_a^2 w + B_1 \left[1 + \frac{\partial w}{\partial x} \right] + C_r \theta - M_a^2 w + B_1 \left[1 + \frac{\partial w}{\partial x} \right] + C_r \theta - M_a^2 w + B_1 \left[1 + \frac{\partial w}{\partial x} \right] + C_r \theta - M_a^2 w + B_1 \left[1 + \frac{\partial w}{\partial x} \right] + C_r \theta - M_a^2 w + B_1 \left[1 + \frac{\partial w}{\partial x} \right] + C_r \theta - M_a^2 w + B_1 \left[1 + \frac{\partial w}{\partial x} \right] + C_r \theta - M_a^2 w + B_1 \left[1 + \frac{\partial w}{\partial x} \right] + C_r \theta - M_a^2 w + B_1 \left[1 + \frac{\partial w}{\partial x} \right] + C_r \theta - M_a^2 w + C_r \theta$$

 $e\cos(c_1t)$],

$$\frac{\partial \theta}{\partial t} = \frac{1}{\Pr R^2(z) Re} \left(\frac{1}{x} \frac{\partial \theta}{\partial x} + \frac{\partial^2 \theta}{\partial x^2} \right) + \frac{Nr}{\Pr R^2(z) Re} \frac{\partial^2 \theta}{\partial x^2} + \frac{Ec M_a^2}{Re} W^2 . \tag{3.24}$$

Or

$$Re\frac{\partial w}{\partial t} = \frac{1}{xR} \left(\frac{1}{R} \frac{\partial w}{\partial x} + B_n \left(1 - e^{-\frac{M}{R} \left| \frac{\partial w}{\partial x} \right|} \right) \right) + \frac{1}{R^2} \frac{\partial^2 w}{\partial x^2} + \frac{B_n M}{R^2} \frac{\partial^2 w}{\partial x^2} e^{-\frac{M}{R} \left| \frac{\partial w}{\partial x} \right|} +$$
(3.25)

$$G_r\theta - M_a^2w + B_1[1 + e\cos(c_1t)]$$
,

$$\frac{\partial \theta}{\partial t} = \frac{1}{\Pr R^2(z) Re} \left(\frac{1}{x} \frac{\partial \theta}{\partial x} + \frac{\partial^2 \theta}{\partial x^2} \right) + \frac{Nr}{\Pr R^2(z) Re} \frac{\partial^2 \theta}{\partial x^2} + \frac{Ec M_a^2}{Re} W^2.$$
 (3.26)

The transformed boundary conditions are:

$$w(x,0) = 0$$
, $\theta(x,0) = 0$, at $t = 0$,

$$\frac{\partial w(0,t)}{\partial x} = 0, \ \frac{\partial \theta(0,t)}{\partial x} = 0, \ at \ x = 0, \tag{3.27}$$

$$w(1,t) = w_s$$
, $\theta(1,t) = 1$, at $x = 1$.

The equations for volumetric flow rate, wall shear stress, and flow resistance are:

$$\tau_{s} = \left(\frac{1}{R}\frac{\partial w}{\partial x} + B_{n}\left(1 - e^{-\frac{M}{R}\left|\frac{\partial w}{\partial x}\right|}\right)\right)_{x=1},\tag{3.28}$$

$$Q_F = R^2 2\pi \int_0^1 w \, x \, dx \, , \tag{3.29}$$

$$\lambda = \frac{L\left(\frac{\partial P}{\partial z}\right)}{O_E} \,. \tag{3.30}$$

3.3 Finite difference approximation

The forward time central space (FTCS) approach is used to compute the partial differential equations numerically. FTCS is utilized because it is simple and reliable in computational fluid dynamics; the procedure first discretises the spatial domain. Subsequently, for each node x_i at time t_j , the velocity component w is computed. The method uses central differencing for the spatial derivatives (second-order accurate) and forward differencing for time to ensure stability and efficiency.

$$\frac{\partial w}{\partial t} \cong \frac{w_{i,j+1} - w_{i,j}}{\Delta t},\tag{3.31}$$

$$\frac{\partial w}{\partial x} \cong \frac{w_{i+1,j} - w_{i-1,j}}{2\Delta x},\tag{3.32}$$

$$\frac{\partial^2 w}{\partial x^2} \cong \frac{w_{i+1,j} - 2w_{i,j} + w_{i-1,j}}{\Delta x^2},\tag{3.33}$$

$$w_{i,j+1} = w_{i,j} +$$

$$\frac{\Delta t \left[B_{1}(1+e\cos(c_{1}t_{j})) + \frac{1}{x_{i}R}\left(\frac{1}{R}w_{x} + B_{n}\left(1 - e^{-\frac{M}{R}|w_{x}|}\right)\right) + \frac{1}{R^{2}}w_{xx} + \frac{B_{n}M}{R^{2}}w_{xx} e^{-\frac{M}{R}|w_{x}|} + G_{r}\theta_{i,j} - M_{a}^{2}w_{i,j}\right]}{Re},$$
(3.34)

$$\theta_{i,j+1} = \theta_{i,j} + \Delta t \left[\frac{1}{\Pr R^2 Re} \left(\frac{1}{x_i} \theta_x + \theta_{xx} \right) + \frac{Nr}{\Pr R^2 Re} \theta_{xx} + \frac{Ec M_a^2}{Re} w_{i,j}^2 \right]. \tag{3.35}$$

With boundary conditions

$$w_{i}^{1} = \theta_{i}^{1} = 0 \text{ at } t = 0 ,$$

$$w_{N+1}^{j} = w_{N}^{j}, \theta_{N+1}^{j} = \theta_{N}^{j} \text{ at } x = 0,$$

$$w_{N+1}^{j} = 0, \theta_{N+1}^{j} = 1, \text{ at } x = 1 .$$
(3.36)

3.4 Stability Criteria

Numerical method starts with spatial domain discretising into N+1 grid points, by taking step size of $\Delta x = 1/(N+1)$. Velocity component is computed over specific

instances t_j at each of these spatial positions, where $t_j = (k-1) \Delta t$ and Δt denotes the time step. The choice of Δx and Δt has a significant impact on the numerical method's stability. Step sizes of $\Delta x = 0.025$ and $\Delta t = 0.00001$ were selected after numerous numerical experiments to ensure a consistent and stable solution.

3.5 Results and discussion

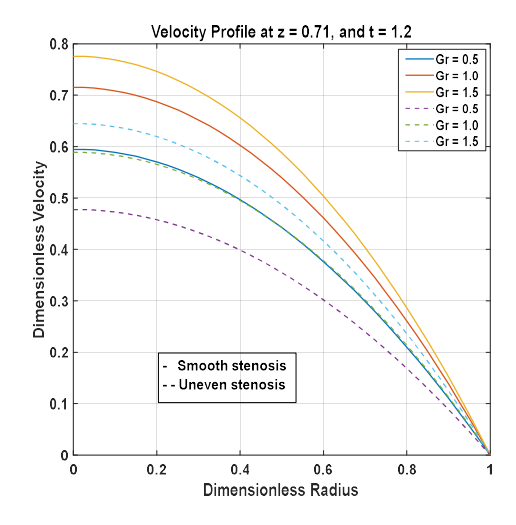
Important simulation parameters is set to presenting the findings. These consist of the following: M=100 (regularization parameter), Pr=21 (Prandtl number), $\delta=0.1$ (stenosis height), Re=0.5 (Reynolds number), Bn=0.01 (Bingham number), and $B_1=2$ (mean pressure gradient). Additional values include: e=0.5 (amplitude of pressure), Ec=0.1 (Eckert number), Ma=0.5 (Hartmann number), Nr=1 (thermal radiation), $R_0=1$ (normal artery radius), L=2 (artery length), and $\alpha=90^\circ$ (angle of the artery). The pressure frequency, $c_1=2\pi$, is time-related quantities. Up until time t=5, $\Delta x=0.025$ and $\Delta t=0.00001$.

Fig. (3.2) shows the dependence of blood velocity on Grashof numbers (Gr). As Gr increases, thermal forces overpower and enhance momentum transfer with enhanced overall fluid velocity. This illustrates how irregularities in the artery wall affect arterial blood flow: smooth stenosis promotes higher flow, whereas uneven stenosis decreases velocity because of increased resistance. With an increase in Gr, thermal buoyancy increases the velocity close to the arterial wall, resulting an increase in wall shear stress as shown in Fig. (3.3), smooth stenosis always produces more shear than irregular stenosis, showing to reduce resistance to flow and improved momentum transfer. The flow rate also improves with Gr can be seen in Fig. (3.4), as smoother stenosis is less resistant as compared to irregular stenosis. On the other hand, Fig. (3.5) indicating that impedance is reducing with increasing Gr, as it varies in inverse proportion to flow rate,

thermal forces assist blood to overcome the constriction more effectively, particularly in smoother geometries.

As the Hartmann number Ma is higher, indicating greater magnetic field influence, the Lorentz force act as a resistive drag on blood flow. This causes the velocity to decrease, as well as reducing wall shear stress, indicated in the Fig. (3.6) and Fig. (3.7) respectively. The total flow rate reduce as the fluid motion dampened by magnetic damping, displayed in Fig. (3.8). As a result, impedance is increased, represented in Fig. (3.9), because the magnetic resistance contributes to the flow blockage, particularly in narrowed arteries, making it more difficult for blood to flow through, even more so in irregular stenosis. Fig. (3.10) and Fig. (3.11) show that as the Bingham number becomes larger, the blood is able to overcome its initial resistance to flow and flows more steadily. This results in increased velocity and less turbulent flow, decreasing overall resistance within the artery, even with stenosis.

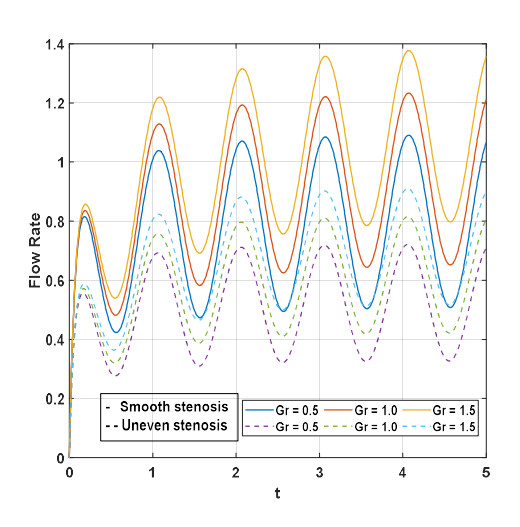
The Fig. (3.12) display impact of thermal radiation on blood temperature within a stenosed artery. With the increase in radiation parameter Nr, temperature profile rises because there is increased radiative heat transfer, which enhances thermal diffusivity by contributing more thermal energy into the system. This temperature rise can also indirectly increase momentum diffusivity by decreasing fluid viscosity. Effect of change of Eckert number on temperature is demonstrated in Fig. (3.13). As indicated from the figure, by increasing Ec, temperature also increasing. In this respect, the Eckert number describes the self-heating of fluid (blood) due to the internal friction of the fluid and ultimately increasing temperature profile of fluid.



2

Fig.3. 2: Velocity profile for *Gr*.

Fig.3. 3: Wall Shear Stress for Gr.



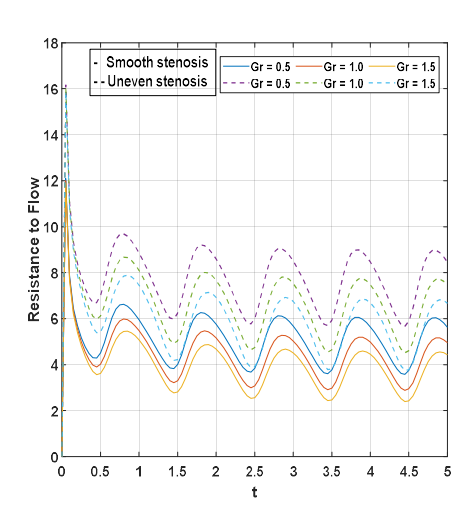


Fig.3. 4: Flow rate for *Gr*.

Fig.3. 5: Resistive impedance for Gr.

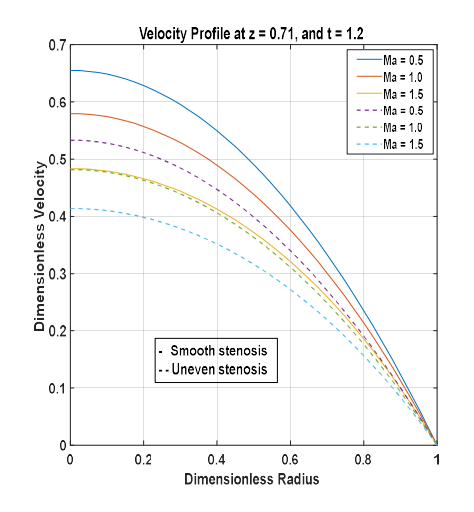
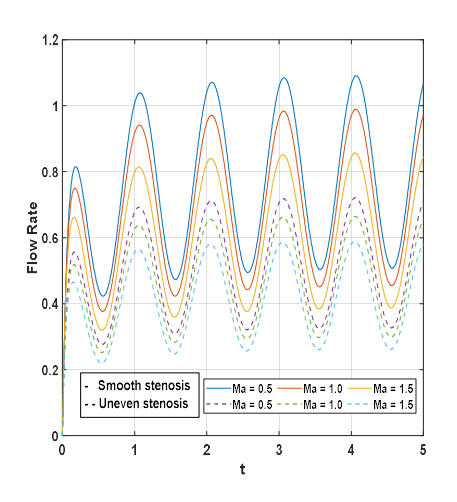


Fig.3. 6: Velocity profile for Ma, Gr = 0.5.

Fig.3. 7: Wall shear stress for $M\alpha$.



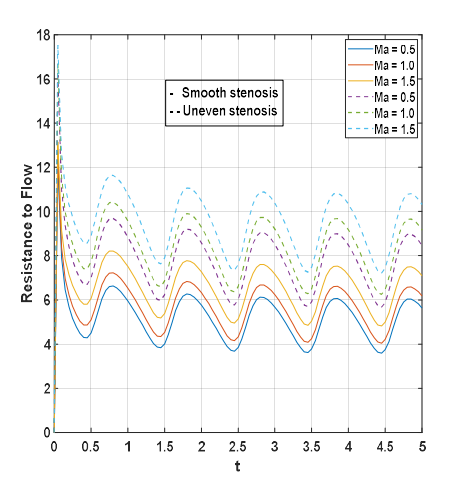


Fig.3. 8: Flow rate for $M\alpha$, Gr = 0.5.

Fig.3. 9: Resistive impedance for Ma.

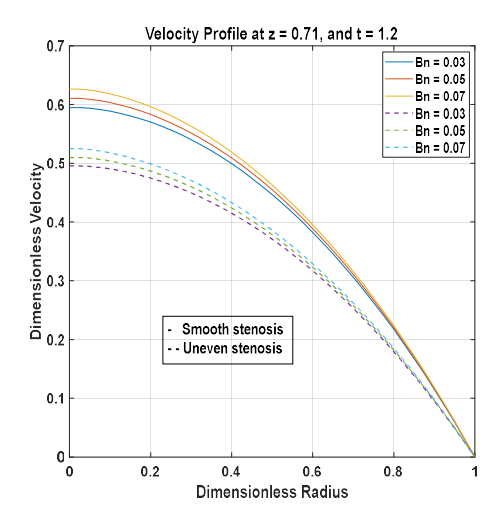


Fig.3. 10: Velocity profile for *Bn*.

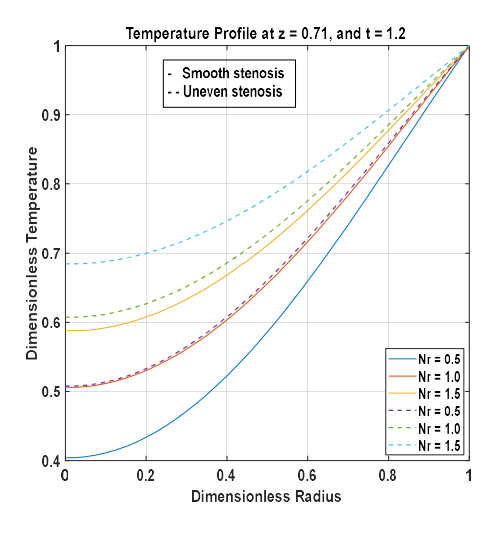


Fig.3. 12: Temperature profile for *Nr*.

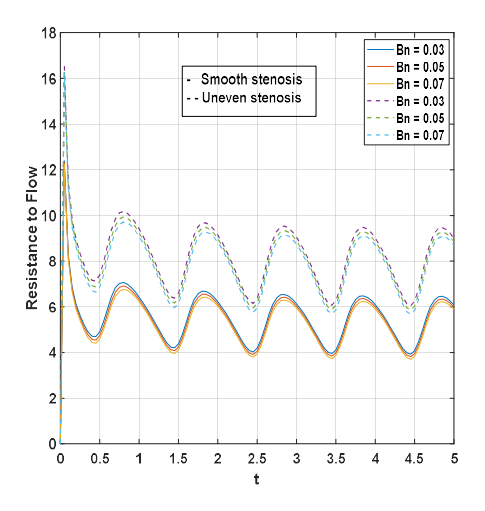


Fig.3. 11: Resistive impedance for Bn.

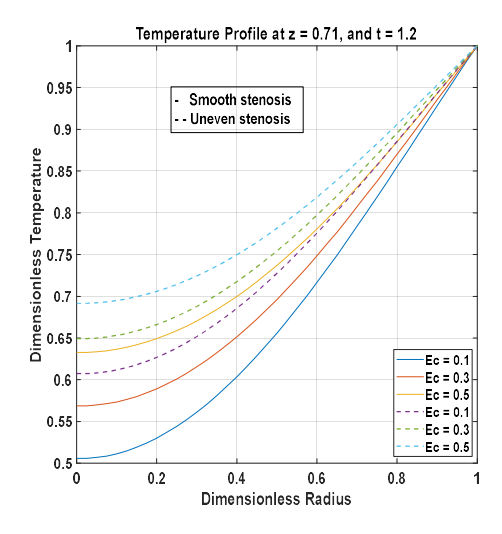


Fig.3. 13: Temperature profile for *Ec*.

3.6 Conclusion

Effect of various parameters on flow dynamics in the artery with smooth and nonsmooth stenosed is explored in this study. The results show the critical roles that thermal and electromagnetic forces play in controlling the blood velocity, temperature, flow rate, wall shear stress, and impedance. The research also considers an unsteady part of the pressure gradient, making it into a more realistic model of blood flow dynamics. The key findings found while exploring them are:

- Raising the Grashof number increases the thermal buoyancy, and this causes increased blood velocity, wall shear stress, and total flow rate, particularly in case of arteries with smooth stenosis.
- Arteries with smooth stenosis are found to offer less resistance and allow for more efficient momentum transfer compared to those with uneven stenosis.
- A more intense magnetic field, which is characterized by a higher Hartmann number, generates Lorentz forces that have the effects of decelerating the flow, decreasing velocity and shear stress, and increasing flow resistance.
- By increasing the Bingham number blood velocity increases, this is because Bingham number helps the blood overcome initial yield stress, which supports a more stable flow through the constricted region.
- Thermal radiation has significantly affected temperature inside the artery, which can reduce viscosity and promote easier blood flow through the stenosed region.

These results help improve our understanding of abnormal blood flow and offer practical insights for doctors to diagnose and manage artery-related health issues.

References

- [1]. Ku, D. N. (1997). Blood flow in arteries. Annual review of fluid mechanics, 29(1), 399-434.
- [2]. Jamil, D. F., Saleem, S., Roslan, R., Al-Mubaddel, F. S., Rahimi-Gorji, M., Issakhov, A., & Din, S. U. (2021). Analysis of non-Newtonian magnetic Casson blood flow in an inclined stenosed artery using Caputo-Fabrizio fractional derivatives. Computer Methods and Programs in Biomedicine, 203, 106044.
- [3]. Patel, H., & Patel, N. (2023). Study of fractional-order model on Casson blood flow in stenosed artery with magnetic field effect. Waves in Random and Complex Media, 1-19.
- [4]. Majeed, S., Ali, F., Imtiaz, A., Khan, I., & Andualem, M. (2022). Fractional model of MHD blood flow in a cylindrical tube containing magnetic particles. Scientific reports, 12(1), 418.
- [5]. Jamil, D. F., Uddin, S., Kazi, M., Roslan, R., Gorji, M. R., & Akhir, M. K. M. (2023). MHD blood flow effects of Casson fluid with Caputo-Fabrizio fractional derivatives through an inclined blood vessels with thermal radiation. Heliyon, 9(11).
- [6]. Tabi, C. B., Ndjawa, P. A., Motsumi, T. G., Bansi, C. D. K., & Kofané, T. C. (2020). Magnetic field effect on a fractionalized blood flow model in the presence of magnetic particles and thermal radiations. Chaos, Solitons & Fractals, 131, 109540.
- [7]. Luqman, M., Iqbal, S., Younas, H. M., Ali, J., Ahmed, N., & Akgül, A. (2020).
 An efficient computational approach for fractional model of blood flow in oscillatory arteries with thermal radiation and magnetic field effects. Available at SSRN 4313039.

- [8]. Yakubu, D. G., Abdulhameed, M., Adamu, G. T., Hassan, U., & Kaurangini, M. L. (2022). Construction of the exact solution of blood flow of Oldroyd-B fluids through arteries with effects of fractional derivative magnetic field and heat transfer. Journal of Mechanics in Medicine and Biology, 22(10), 2250068.
- [9]. Kot, M. E., & Elmaboud, Y. A. (2024). Numerical simulation of electroosmotic sutterby hybrid nanofluid flowing through an irregularly mild stenotic artery with an aneurysm. Arabian Journal for Science and Engineering, 49(2), 2483-2498.
- [10]. Raju, C. S. K., Basha, H. T., Noor, N. F. M., Shah, N. A., & Yook, S. J. (2024).
 Significance of body acceleration and gold nanoparticles through blood flow in
 an uneven/composite inclined stenosis artery: A finite difference
 computation. Mathematics and Computers in Simulation, 215, 399-419.
- [11]. Abbas, Z., Shabbir, M. S., & Ali, N. (2018). Numerical study of magnetohydrodynamic pulsatile flow of Sutterby fluid through an inclined overlapping arterial stenosis in the presence of periodic body acceleration. Results in Physics, 9, 753-762.
- [12]. Akbar, N. S. (2015). Biomathematical study of Sutterby fluid model for blood flow in stenosed arteries. International Journal of Biomathematics, 8(06), 1550075.
- [13]. Fry, D. L. (1968). Acute vascular endothelial changes associated with increased blood velocity gradients. Circulation research, 22(2), 165-197.
- [14]. Ku, D. N., Giddens, D. P., Zarins, C. K., & Glagov, S. (1985). Pulsatile flow and atherosclerosis in the human carotid bifurcation. Positive correlation between plaque location and low oscillating shear stress. Arteriosclerosis: An Official Journal of the American Heart Association, Inc., 5(3), 293-302.

- [15]. Padmanabhan, N., & Devanathan, R. (1981). Mathematical model of an arterial stenosis, allowing for tethering. Medical and Biological Engineering and Computing, 19, 385-390.
- [16]. Mehrotra, R., Jayaraman, G., & Padmanabhan, N. (1985). Pulsatile blood flow in a stenosed artery—a theoretical model. Medical and Biological Engineering and Computing, 23, 55-62.
- [17]. Batchelor, G. K. (2000). An introduction to fluid dynamics. Cambridge university press.
- [18]. Papanastasiou, T. C. (1987). Flows of materials with yield. Journal of rheology, 31(5), 385-404.
- [19]. Mandal, P. K. (2005). An unsteady analysis of non-Newtonian blood flow through tapered arteries with a stenosis. International journal of non-linear mechanics, 40(1), 151-164.
- [20]. Tripathi, J., Vasu, B., & Bég, O. A. (2021). Computational simulations of hybrid mediated nano-hemodynamics (Ag-Au/Blood) through an irregular symmetric stenosis. Computers in Biology and Medicine, 130, 104213.
- [21]. Handford, S. W. (1965). Physiology and Biophysics of the Circulation: An Introductory Text, 394-394.